Emulsification of Supersaturated Solutions Amplifies Induction Time Variation in Crystallization

Anish V. Dighe, Prem K.R. Podupu, Meenesh R. Singh*

Department of Chemical Engineering, University of Illinois Chicago, Chicago, IL 60607, United States

Submitted to Crystal Growth & Design

Corresponding Author:

Prof. Meenesh R. Singh Associate Professor Department of Chemical Engineering 929 W. Taylor St University of Illinois Chicago Chicago, IL 60607 Tel: (312) 413-7673

Email: mrsingh@uic.edu

Keywords: Induction Time, Brownian Dynamics, Density Distributions, Time Scale Analysis

Abstract

The induction time for the onset of nucleation is known to decrease with increasing solution supersaturation. A large variation in induction time is experimentally observed for various organic crystals, whose origin is often associated with the stochastic nature of the nucleation process. Although several empirical models for induction time and nucleation rate have been developed, they remained highly unreliable, with model predictions differing by orders of magnitude from experimental measurements. A satisfactory explanation for the induction time variation has not been developed yet. We report here that the variations in induction times can be attributed to a previously unrecognized consequence of the phaseseparation or emulsification of supersaturated solution, in addition to the effect of stochastic nucleation. A large-scale Brownian dynamics simulation of antisolvent crystallization of histidine in a water-ethanol mixture is performed to demonstrate the mechanism of microphase/emulsion formation in supersaturated solutions and its consequence on induction time variation. Furthermore, we show that the average induction time depends on supersaturation, and the supersaturation-dependent diffusion of histidine molecules governs the stochastic nature of the induction time. Moreover, at varying supersaturations, the likelihood of forming stable and metastable polymorphs of histidine was estimated. This approach provides valuable insights into the crystallization behavior of histidine and predicted induction time reasonably matches the experimentally observed induction time.

1. Introduction

Understanding the role of the solvent environment and dynamics of solute-solvent interactions enable efficient synthesis of crystalline materials using the process of crystallization.¹ The process of crystallization is versatile and is applied to synthesize diverse types of materials.²⁻⁵ However, the underlying stochastic nature of the intricacies involved in the process results in variation in the induction time of crystallization and, in turn, affects the outcome of crystallization.^{6, 7} This variation at the same operating conditions is commonly observed for crystallization processes that involve the non-covalent self-assembly of molecules.⁸ Furthermore, the stochastic nature of the nucleation also leads to variations in induction times for the formation of crystal nuclei.^{9, 10} The relationship between induction time, solute-solvent interactions, and the local solvent environment is not fully understood.

The change in the induction time of the crystallization process is attributed to the changes in local supersaturation. Variations in local supersaturation, caused by the Brownian motion-driven local fluctuations of solute concentrations and temperature¹¹, affect the nucleation and growth rates of crystals.¹² The empirical correlations of the inherent rates and the supersaturation are commonly used to control the crystallization process.¹³ However, such an approach relies on average properties and does not account for deviations due to local density differences. Previously, it has been shown that local density and temperature fluctuations affect the growth rates of crystals.¹¹ The effect of diffusion on the local density of solute molecules has also been previously considered. Such studies rely on the assumption that growth units are spherical, which is most commonly a case for the crystallization of nanocrystalline materials.^{14, 15} None of the studies have predicted the induction time. Furthermore, a large number of molecules involved in

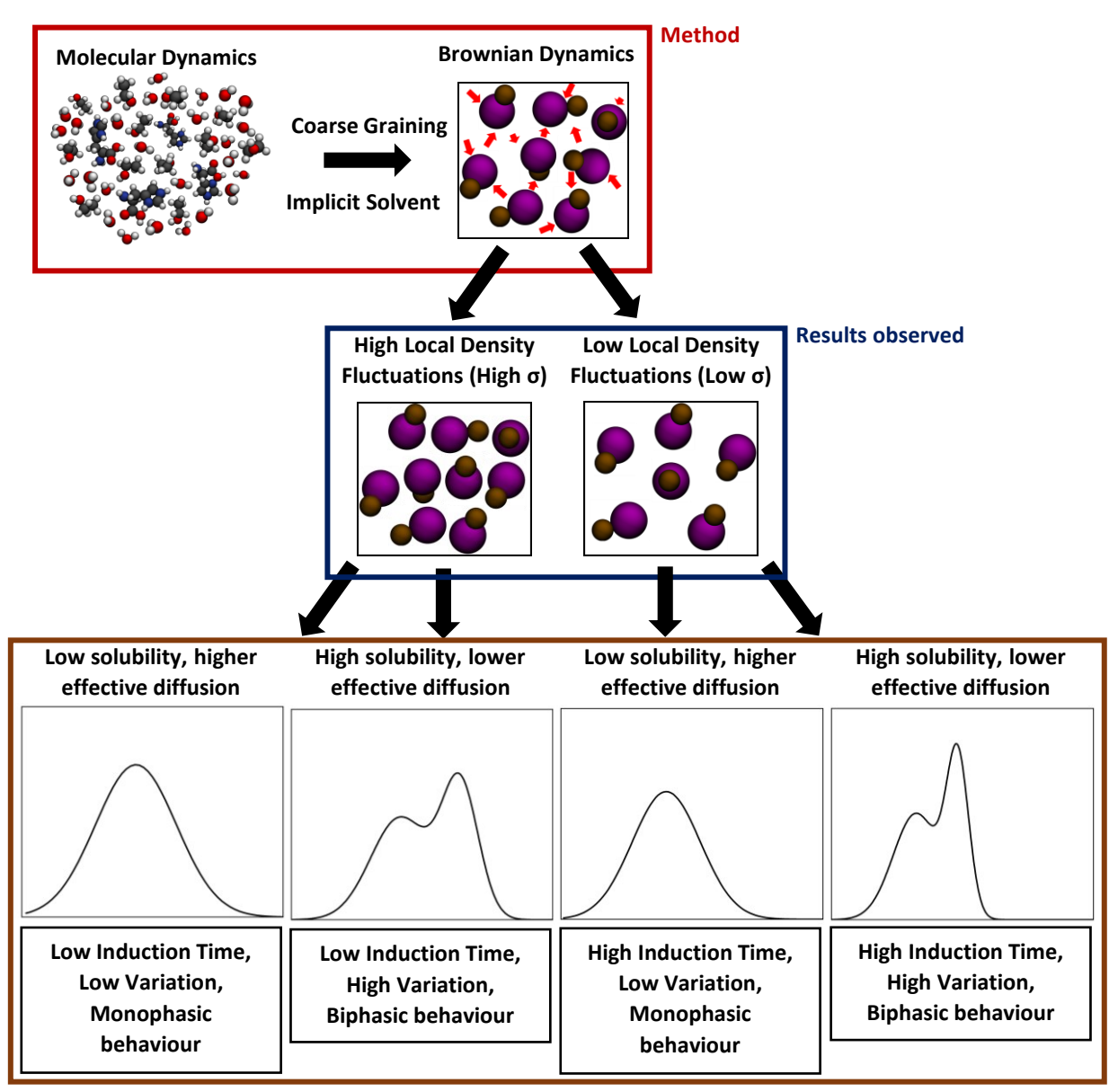
the formation of the critical nucleus and their non-equilibrium behavior add more complexity to the problem. Hence, it is necessary to build a computational framework that considers the underlying molecular attachment events that lead to nucleation (referred to as "events" from here on) and gain mechanistic insights into such events that occur over longer timescales.

The theoretical and experimental methods to understand the induction time and its relationship to supersaturation are motivated based on empirical correlations and classical nucleation theory. ^{16, 17} Most commonly, a large number of experiments are performed, and the experimental results are fitted to the empirical model to obtain the values of the parameters involved. In the case of limited experimental data, a large-scale parameter search is performed to determine the values of the parameters involved. ¹⁸ Furthermore, experimental methods have evolved that allow continuous crystallization at constant supersaturations using microfluidic devices. ¹⁹⁻²¹ Although such methods have allowed greater control over the crystallization process, the mechanistic details are still unknown.

The computational approaches aimed at understanding the non-covalent self-assembly of relatively larger molecules rely on coarse-graining approaches. ²²⁻²⁴ Colloidal or polymeric particles are coarse-grained into simpler geometric shapes that reduce the number of degrees of freedom. ²⁵⁻²⁹ Such reduction in the degrees of freedom coupled with the use of scaled variables allows large-scale simulations that can simulate crystallization using techniques such as Molecular Dynamics (MD), Brownian dynamics (BD), and kinetic Monte-Carlo techniques. ³⁰⁻³² However, the parameterization of the force fields and the validation of the results obtained from such simulations is not trivial. Such explicit molecular simulations of inorganic and small organic molecules have also been performed. These simulations have estimated the energy change required for the formation of crystals but are limited to smaller timescales and a lower number of molecules in the simulation box. ^{33, 34}

We use a coupled approach of molecular dynamics and Brownian dynamics to gain mechanistic insights over longer timescales and maintain the information obtained from smaller timescale events. The molecular dynamics simulations of histidine antisolvent crystallization were performed at various mole fractions of ethanol (xeth) (in the ethanol-water mixture) and supersaturation ratios (σ) with water and ethanol as solvent and antisolvent, respectively. Histidine has two polymorphs – stable polymorph A and metastable polymorph B. 16 With the help of a semi-classical double-well approach, the activation energy of histidine molecules at the transition state was calculated. The configuration at the transition state was also used to explore the energy landscape at various supersaturations to understand the probability of forming stable and metastable polymorphs. The MD simulation details and the details of the calculation of the energy landscape are given in Sections S1 and S2 of the supporting information, respectively. Furthermore, the position and velocity of histidine molecules were analyzed, and the information was then used to obtain drift and diffusion terms for the Brownian dynamics simulations scheme. The histidine molecule was coarse-grained into two beads connected for the BD simulation framework. The BD simulation was performed to calculate the position of the center of mass of the beads as a function of time.³⁵ The BD simulation details are given in Section S3 of the supporting information. The trajectories of BD simulations were then analyzed to calculate the

local fluctuations in the supersaturation, understand the timescale of polymorph-specific events, and calculate the induction time. **Figure** 1 summarizes the work performed in this article.



Monophasic and biphasic behaviour that results in variations in induction time

Figure 1: Overview of the method used to relate molecular events to the induction time of histidine antisolvent crystallization. Molecular dynamics simulations were performed to understand the dynamics of solute-solvent-antisolvent interactions and to calculate the activation barrier for the growth of crystals. Histidine molecules were coarse-grained into two beads connected to each other. The position and velocity obtained from MD simulations were used to simulate the center of mass of coarse-grained Histidine molecules using BD simulations. The BD simulation reveals the monophasic and biphasic behavior of molecular self-assembly, which is then related to the fluctuations in the induction time.

2. Methods

Molecular Dynamic (MD) simulations of histidine in solvent/antisolvent mixture were performed using GROMACS³⁶, a high-performance molecular dynamics package. We performed 24 simulations, that included ethanol mole fractions of 0 to 0.5 and the corresponding supersaturation values of 1.2, 1.5, 2 and 2.5. Supersaturation ratio is defined as the ratio of the concentration of solute in the solvent/antisolvent mixture to the saturation concentration of solute in the solvent/antisolvent mixture at a given temperature. Additional information about these MD simulations, the theoretical and experimental solubilities (**Table S1** of the supplementary information), as well as information on trajectory analysis, is provided in **Section S1** of the supplementary information. Secondly, the transition state and the energy of transition were calculated based on the double-well approach, which was further used to calculate the interaction energy landscapes as explained in **Section S2** of the supporting information. Finally, the mean square displacement and velocity correlation functions were analyzed from the MD simulations and further used to develop a Brownian Dynamics simulation scheme as described in **Section S3**. The output from the MD simulations was used to develop the coarse-grained model for BD analysis. The overall flowchart of the method is shown in **Figure S1**.

3. Results and Discussion

Molecular dynamics simulations at different mole fractions and supersaturations were performed. The activation energies for the attachment of histidine molecules were calculated. The polymorph-specific events were identified with the help of MD simulations. Histidine molecules were classified into two states – (i) fully solvated and (ii) partially desolvated. The classification into either of the thermodynamic states of the histidine molecule (fully solvated or partially desolvated) was based on the number of solvent (water) molecules in the solvation shell of histidine and the pairwise distance between solute molecules. The solvation shell thickness of histidine was found to be 0.63 nm.³⁷ The transition state and the activation barrier required to achieve the transition state is calculated using the semi-classical double-well approach (Figure S2). The transition state is the step before the integration of molecules into crystal surface. To understand the most likely polymorph obtained after transition, we plotted the interaction energy landscapes. The interaction energy landscape is obtained by calculating energy of all possible configurations of transition state. The interaction energy is the total contribution of van der Waals and electrostatic energies. Such an approach has been previously used for cooling crystallization of glutamic acid molecules^{34, 38} and antisolvent crystallization of histidine molecules. However, the interaction energy landscape of histidine is not yet reported in the literature. Figure 2 shows the interaction energy landscape of histidine molecules. The interaction energy landscape shows the most likely configuration of histidine molecules after the transition state is achieved. The color map represents the energy values at every rotation of the histidine molecules. The x- and y- axes are chosen so that every configuration will has a unique position on the energy surface.

The structural similarity region, shown by dashed curves on the energy landscape, is calculated by comparing the all-atom theoretical structures with the experimentally obtained crystal structures of the two polymorphs of histidine.³⁹ Further details of such calculations are

given in **Section S2** of the supplementary information. In the energy landscapes of low supersaturations (σ) of 1.2 and 1.5, shown in **Figure 2a-2b**, the global minimum in the energy landscape is enveloped by the similarity region of stable polymorph A. Arrows indicate the locations of the global minimum. It agrees with the experimental evidence that at low supersaturations, stable polymorph is obtained as the crystallization outcome. The global minimum is enveloped by the metastable polymorph B at high supersaturations of 2 and 2.5, shown in **Figure 2c-2d**. These computational calculations agree with the experimental observation that the metastable polymorph B is crystallized at high supersaturation values. The interaction energy landscapes allow the calculation of polymorph-specific probability as a function of supersaturation. The probability was calculated based on the ratio of the weighted average of the number of low-energy regions enveloped by the similarity region of the specific polymorph and the weighted average of all the low-energy regions. The polymorph-specific probability as a function of supersaturation is shown in **Figure S3** of the supporting information.

The interaction energy landscape yields configuration-specific information that leads to either histidine polymorph. The brownian dynamics simulation method was used to understand the dynamics of histidine molecules at a longer timescale using a higher volume of the simulation box. Traditionally, the drift and diffusion terms of the Brownian dynamics equation are calculated by coarse-graining the molecule under consideration and then applying the force balance to derive a Fokker-Planck-like diffusion equation. In this case, based on the geometry of the individual histidine molecule, the histidine molecule is coarse-grained into two spherical beads joined together. The Brownian dynamics simulation scheme is then derived using the trajectories of the MD simulation to solve for the center of mass of the coarse-grained histidine molecule. The validation against MD trajectories is performed by analyzing mean squared displacement (MSD) and velocity autocorrelation (VAC) functions.

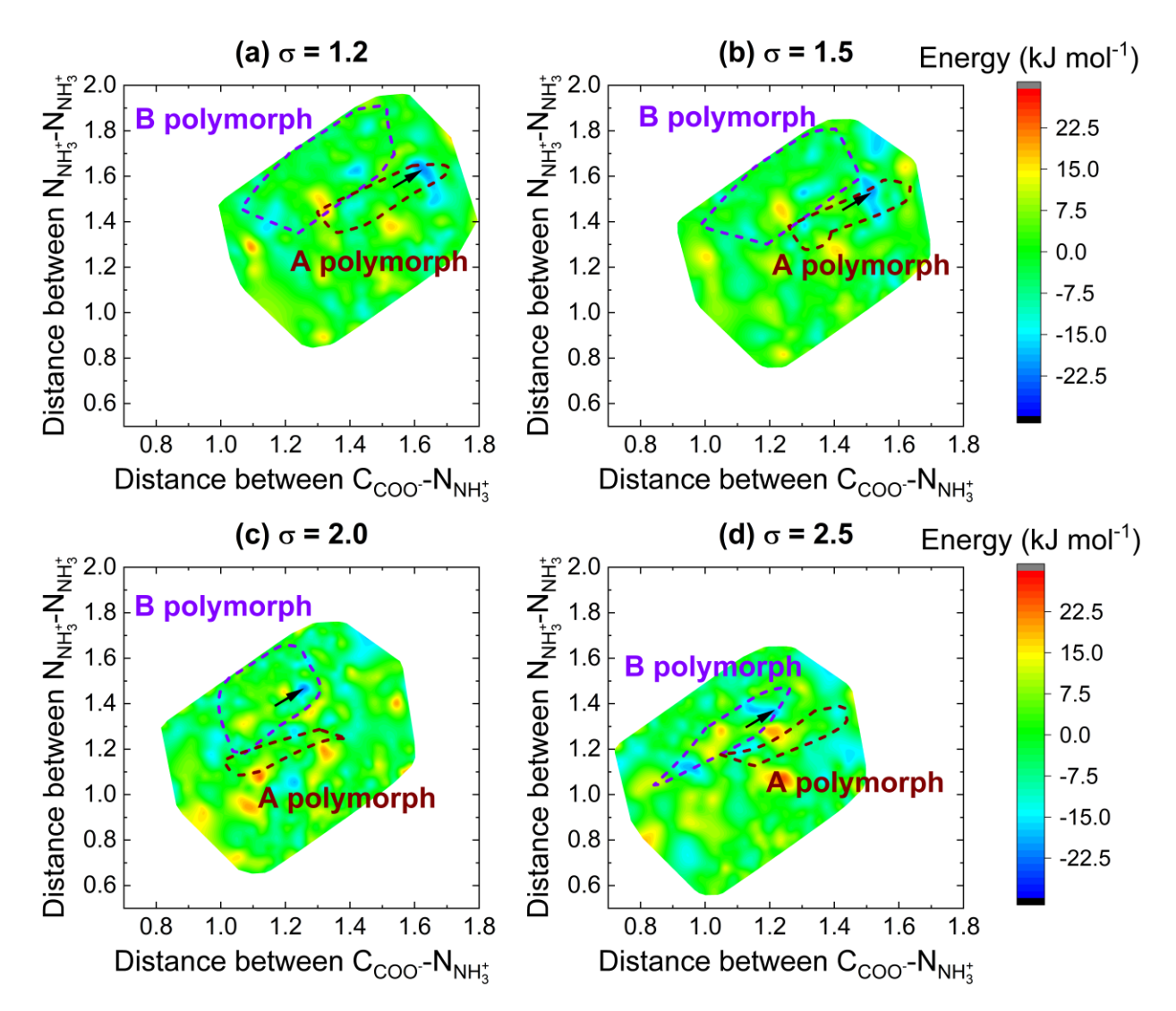


Figure 2: Interaction energy landscape of histidine as a function of supersaturation (σ). (a) $\sigma = 1.2$, (b) $\sigma = 1.5$, (c) $\sigma = 2$, and (d) $\sigma = 2.5$. Distances are given in nm, and the scale bars show the energy of interaction between the configurations at the transition state. Regions inside the dashed curve have theoretical crystal structures similar to that of the experimentally observed ones. The dashed brown curve shows the similarity region of the stable polymorph A, and the dashed violet curve represents the similarity region of the metastable polymorph B. Arrows point to the global minima of the energy landscape.

The validation of BD simulation against MD simulation trajectories is shown in **Figure 3a-c**. The analysis simulations performed at $x_{eth} = 0.5$ and $\sigma = 1.2$ are shown here as it effectively captures the effect of antisolvent. The change in the MSD of the histidine molecule as a function of time is linear, as shown in **Figure 3a**, indicating that the histidine molecule is undergoing pure diffusion. This result is significant because it validates the most common experimental observation that solute molecules mostly undergo pure diffusion during crystallization regardless of supersaturation. Furthermore, based on the fitting of the diffusion coefficient as a function of

 x_{eth} and σ shown in **Figure 3c**, the local solvent-antisolvent environment changes the effective diffusion coefficient.

Simulating the diffusion of the particles using the Brownian dynamics simulation scheme also requires that the Gaussian random process effectively captures the effect of the solvent environment. The impact of the solvent environment on the velocity of histidine molecules is understood with the help of velocity autocorrelation (VAC) functions. VAC is calculated by averaging the velocity at different time step values and yields insights into the average motion of molecules over time scales (Section S3). VAC is shown in Figure 3b for $x_{eth} = 0.5$ and $\sigma = 1.2$. The average of VAC, regardless of the timestep given on the x-axis, is around zero. It implies that the drift function is equal to zero, and the diffusion function of the Brownian dynamics simulation scheme should be a local supersaturation-dependent diffusion coefficient. Also, this result indicates that the velocity of histidine molecules does not depend on the previous timestep and the effect of forces can be modeled with the help of a Gaussian random process with a mean of zero. The MSD analysis and VAC analysis together suggest that the motion of histidine is Brownian motion. Hence, the Brownian dynamics simulation scheme can be effectively applied to understand the dynamics of histidine crystallization at longer timescales.

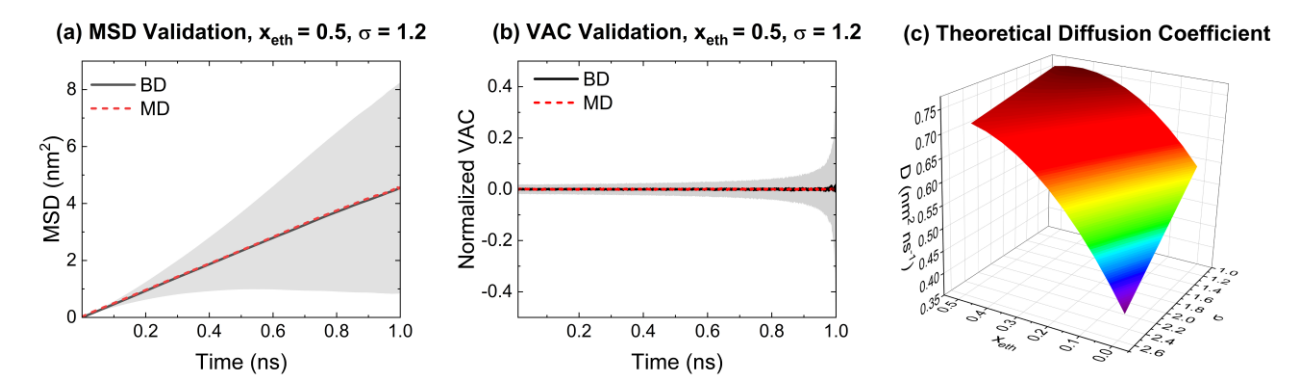


Figure 3: Validation of the BD simulation against mean squared displacement (MSD) and velocity autocorrelation (VAC) function obtained from the MD simulation trajectories and the theoretical diffusion coefficient. (a) MSD Validation, $x_{eth} = 0.5$, and $\sigma = 1.2$, (b) VAC Validation, $x_{eth} = 0.5$, and $\sigma = 1.2$, and (d) Theoretical effective diffusion coefficient. In panels (a) and (b), the solid black line represents the results obtained from the BD simulation, the dashed red line represents the results obtained from the MD simulations, and the shaded portion represents the standard deviation of BD simulation results.

The Brownian dynamics simulation scheme was used to simulate the motion of histidine molecules with higher box volume and a greater number of molecules in the simulation box as per the desired concentration. The number of molecules in the BD simulations is scaled based on previously reported values.³⁷ Higher box volume allows dividing the simulation box into smaller bins to effectively analyze the local concentration experienced by each histidine molecule. Such analysis yields the local distribution of the supersaturation. This analysis is shown in **Figure 4**. The supersaturation distributions yield mechanistic insights into the process of antisolvent crystallization. Increasing x_{eth} at constant σ , as shown in **Figure 4a**, or increasing σ at constant σ as shown in **Figure 4b**, depicts the variations in frequency (of events leading to

crystallization) caused by the effect of decreasing diffusion coefficient. However, the distribution of local supersaturation is significantly different. In all the cases, the distribution average is the supersaturation value the simulation box represents. It can be seen that, even in the extreme case of $x_{eth} = 0.5$ and $\sigma = 2.5$ considered in this article, some of the histidine molecules experience an undersaturated local environment. At $x_{eth} = 0$ and $\sigma = 1.2$, the distribution of the supersaturation has two peaks. The initial peak represents the molecules that are undersaturated. Although the overall box is supersaturated, the solute molecules are experiencing two distinct thermodynamic states locally. Such biphasic behavior is experimentally observed for some crystallization systems. 40, 41 As xeth increases, the distribution becomes wider such that two distinct peaks disappear, indicating that the number of events where molecules experience an undersaturated local environment has decreased. In Figure 4a, the case of $x_{eth} = 0.5$ has the widest distribution. However, as supersaturation increases, as shown in Figure 4b, the two peaks reappear, indicating that the effect of an increase in supersaturation is not uniform across the simulation box. Such observation also explains the empirical statement that it is difficult to control the process of crystallization at high supersaturations⁴². Although the average supersaturation of the box is around 2.5, there are a significant number of events (> 45%) where histidine molecules do not experience the local environment of supersaturation is 2.5.

The emulsification or biphasic behavior, elucidated in **Figure 4c**, is more pronounced at lower mole fractions and supersaturations. As the mole fraction of ethanol increases, the solute molecules experience more uniform supersaturation across the simulation box. Such transitions from biphasic to monophasic behavior, as shown in **Figure 4a**, explain the experimentally observed exponential changes in the induction times at the same supersaturation but varying mole fractions. Particularly, for histidine, the induction time is around a few hours at low mole fraction values. However, induction time reduces to a few seconds as the mole fraction increases. This biphasic behavior can be attributed to the concentration-dependent diffusion coefficient of the histidine molecules. Higher concentration reduces the effective diffusion coefficient, which in turn results in higher time required to achieve local supersaturation equal to the bulk supersaturation. If the simulations where the local supersaturation distribution has two peaks are performed for much longer times, then the peak farther away from the bulk supersaturation value would vanish and make the distribution of local supersaturation sharper.

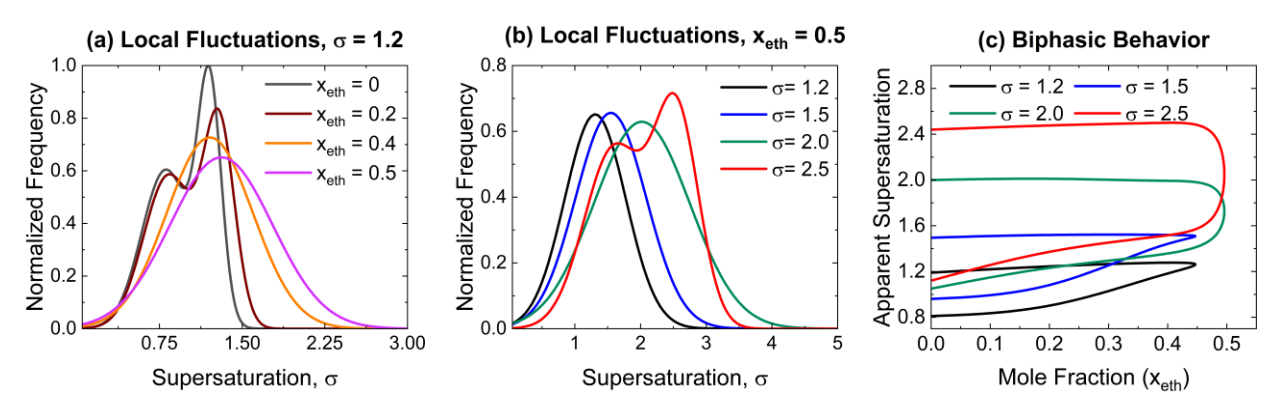


Figure 4: Analysis of local fluctuations in supersaturation and time span of the events leading to polymorph formation. (a) Local fluctuations in supersaturation as a function of x_{eth} at constant

bulk supersaturation ratio $\sigma = 1.2$, (b) local fluctuations in supersaturation at various bulk supersaturation ratios (σ) at constant $x_{eth} = 0.5$, and (c) elucidation of biphasic behavior due to local fluctuations.

The formation probability obtained from the interaction energy landscape analysis can be used to apply boundary conditions in the BD simulation. At any event, when two molecules are in a favorable configuration for the formation of either polymorph, a random number is generated and compared to that of formation probability to check if the event leads to crystal formation. Without such boundary conditions, results are purely based on kinetics (motion). The boundary conditions based on the probability allow consideration of crystal structure formation energetics during the BD simulation. The results for both cases are shown in **Figure S4** of the supplementary information. In both cases, the number of kinetic events leading to stable polymorph A formation is the highest. However, energetics play an essential role- as the supersaturation increases, the energetic contribution required for the formation of the stable polymorph A increases, thus leading to a lower number of events of polymorph A at higher supersaturation. A transition point where the number of events leading to the formation of both polymorphs is almost equal occurs at the supersaturation value of 1.6. The results depicted in these figures are obtained from BD simulation of up to 0.1 µs and with a timestep of 1 ns.

The Brownian dynamics simulations also allow calculating the timespan of each event that the histidine molecule is experiencing. For the formation of a crystal, it is necessary that the histidine molecules experience a local environment favorable for crystallization for a time greater than the characteristic time. The characteristic time is the inverse of the rate constant of the molecular attachment. The rate constant values were calculated with the help of the transition state theory, and the activation barrier was calculated from the semi-classical double-well approach. The details of these calculations are given in Section S4 of the supplementary information. At every time step during the simulation, the local supersaturation values and the lifespan (retention time) of each local supersaturation event is stored. The lifespan of each event is then compared with the characteristic obtained from the rate constant values. The configuration information leading to specific polymorphs obtained from energy landscape (Figure 2) analysis coupled with the characteristic time required for the formation of polymorph allows counting the events feasible for the formation of crystal. Figure 5a-5b show the events leading to metastable polymorph B at low ($\sigma = 1.2$) and high ($\sigma = 2.5$) supersaturations. The pink shaded represents the characteristic time of formation of polymorph B at $\sigma = 1.2$ and is given as a reference. As supersaturation increases, the characteristic time decreases. The curves show the distribution of the lifetime of the events that represent the formation of polymorph B. At $x_{eth} = 0$, the characteristic timescale is significantly higher, indicating that it is difficult to crystallize polymorph B at low supersaturation. As the supersaturation increases, the number of events and their lifetime also increases. In the case of $x_{eth} = 0.5$, the characteristic time is lower, indicating that achieving the transition state is the only rate-limiting step, and the energetics of the crystal structure formation will most likely govern the crystallization outcome. It also further indicates that the induction time is lower when histidine is crystallized at higher values of xeth. The empirical observation validates this result that induction time for crystallization of histidine at lower x_{eth} (~0.1) is reported to be in hours, and at higher x_{eth} (~0.1) is reported to be in minutes.

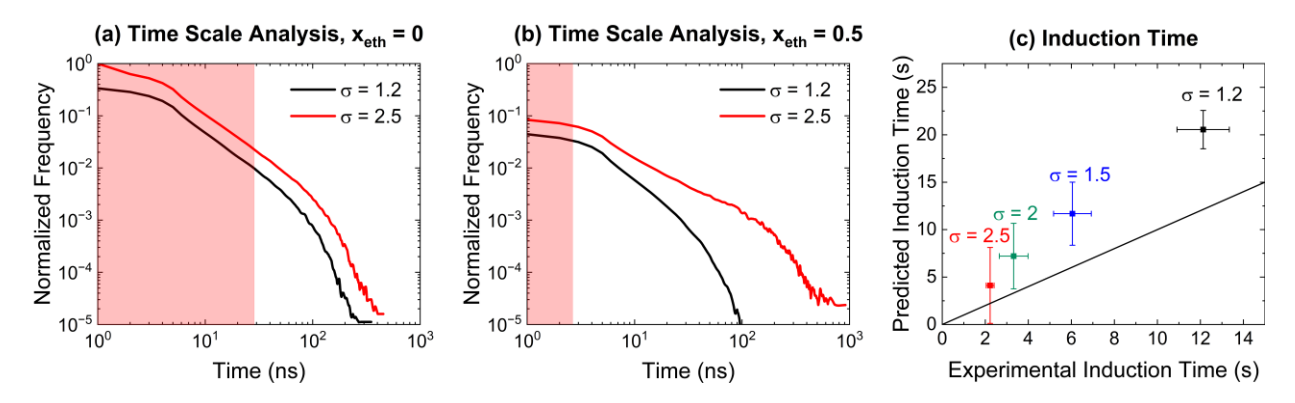


Figure 5: Frequency of events leading to crystallization based on kinetics and energetics of the histidine molecules and predicted induction times plotted against the experimentally observed induction times. (a) frequency of events leading to crystallization at $x_{eth} = 0$, (b) frequency of events leading to crystallization at $x_{eth} = 0.5$, and (c) predicted vs. experimentally observed induction times. The solid black line in panel (c) is the reference line where the predicted induction time equals the experimentally observed induction time.

Experimental induction times and critical nuclei sizes were obtained from the literature.⁹, ⁴³ In the literature, the critical nuclei sizes are reported as the thickness (in nm) of growth units based on the unit cell of histidine.³⁷ These thickness values are used to calculate the volume of growth unit at each supersaturation, which in turn denotes the number of histidine molecules required to form the critical nucleus. The induction time is then calculated as the time needed to achieve the number of attachment events leading to crystal structure formation equal to the number of histidine molecules in the critical nucleus. The predicted induction time is higher than the experimentally observed induction time. One of the reasons could be the under prediction of the rate of attachment. When two monomers surrounded by a solvation shell interact substantially, a more significant number of solvent molecules must be removed from the shell than when a monomer interacts with a crystal nucleus containing a smaller number of solvent molecules. The present work is limited to the combination of two monomers, which has relatively higher energy than a monomer attaching to a crystal nucleus and is, therefore the reason for the longer estimated induction time. Additional discrepancies can occur due to numerical error from multiple sources: (i) MD simulation trajectory fluctuations, (ii) coarsegraining for BD simulations, or (iii) critical nuclei size calculations. However, the timescale of the crystallization of histidine is effectively captured in this approach.

The information about induction time from previous results is summarized in **Figure 6**. Empirically, supersaturation is a measure of the chemical potential of the solution. However, for the formation of crystal nuclei, it is also necessary for histidine molecules to diffuse, form a dense phase, and nucleate into crystals. As the mole fraction of ethanol increases, the number of solute molecules in the simulation box also decreases (**Table S2**). It results in solute molecules having a higher effective diffusion coefficient (D_e). Hence, at high mole fraction and low supersaturation, the number of molecules experiencing local supersaturation closer to bulk supersaturation is higher. At constant mole fraction, as supersaturation raises, it again increases the D_e of histidine molecules resulting in a broad distribution of local supersaturation centered around the bulk supersaturation value (**Figure 4**). The change in the diffusion coefficient affects

the lifespan of the histidine molecule clusters that are necessary to form crystal nuclei (**Figure 5**). The diffusion coefficient dictates the uncertainty in the induction time (**Figure 6a**), while the bulk supersaturation dictates the average induction time (**Figure 6b**).

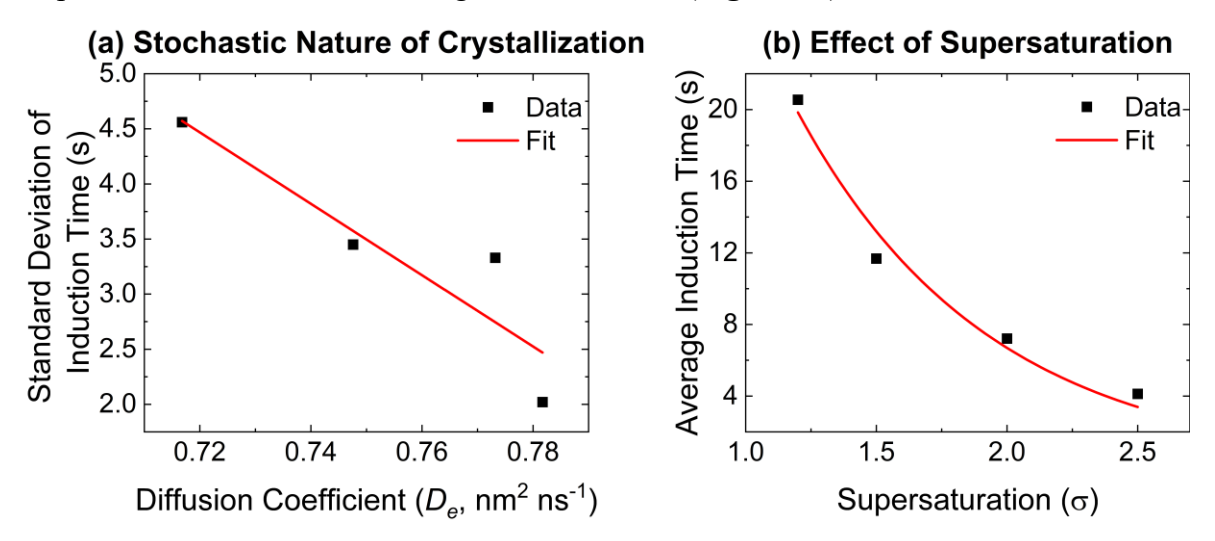


Figure 6: Molecular origins of the induction time. (a) Stochastic nature of crystallization arising due to the diffusion of molecules during the crystallization process and (b) Effect of supersaturation on induction time.

4. Conclusion

The results presented connect the variations in local concentration to the measurable quantities such as supersaturation and induction time. We have shown that the emulsification, the formation dense microphases that are distinct from average bulk phase during crystallization affect the crystallization outcome. The study presented in the article uncovers the relationship between the inherently stochastic nature of nucleation and the kinetics and energetics of molecular motion during the self-assembly process. The diffusion of molecules and the local and bulk supersaturation values affect the self-assembly of molecules during the process of crystallization. The diffusion coefficient dictates the distribution of local supersaturation, which in turn impacts the lifespan of the events leading to the formation of crystals. The bulk supersaturation dictates the chemical potential of the solution, which affects the average induction time of crystallization.

The critical information from each step of the method is captured and implemented in the further stages to retain the necessary features. In the initial step, the semi-classical double-well approach captures the transition state, and the interaction energy landscape yields polymorph-specific configuration information. In the final step, BD captures the local variations in supersaturation and the probable crystallization outcome based on the energy landscape from the previous step. Importantly, it is shown that the molecules with lower molecular weight can be simulated using the BD simulation approach. The position and velocity fluctuations are essential to understand if the BD simulation approach is valid.

The longer timescale simulations yield mechanistic insights into the local environment experienced by the solute molecule. The volume of the simulation box considered in this study is much smaller than that of a real crystallizer. Yet, it is seen that a significant fraction of molecules does not experience the local environment with supersaturation equal to or higher than the average supersaturation represented by the concentration of the simulation box. The lower supersaturation results attachment events that occur at timescale smaller than the characteristic time for the formation of crystals. The addition of antisolvent helps reduce the characteristic time required for crystal formation. However, a higher concentration of antisolvent and higher supersaturation leads to broad asymmetric distribution of local supersaturation. All of the observations together explain the inherently stochastic nature of the process of crystallization.

The energetic contribution incorporated into the BD simulation framework uncovers the transition point near the supersaturation value of 1.6. Furthermore, such BD simulation coupled with classical nucleation theory allows the calculation of induction times using only computer simulation. The predicted induction time reasonably matches the experimental induction time, given the numerical errors arising from various steps in the simulation framework. The conclusions stated in the article together point to the necessity of crystallization control strategies that take into account the local fluctuations in the concentration of the crystallizer.

Supporting Information

Details of the molecular dynamics simulation results, double-well potential and energy landscape calculations, velocity autocorrelation and Brownian dynamics (BD) simulation details, and calculation of characteristic time are provided in the supporting information.

Acknowledgments

This material is based on the work performed at the Materials and Systems Engineering Laboratory at the University of Illinois, Chicago (UIC). M.R.S. acknowledges funding support from UIC and the US National Science Foundation (NSF, EFRI 2132022).

Competing Interests:

The authors declare that there are no competing interests.

Author Contributions:

M.R.S. conceptualized research; M.R.S., A.V.D., and P.K.R.P. designed methodology, AV.D., and P. K. R. P., performed theoretical investigation, A.V.D., P.K.R.P., and M.R.S. performed validation; M.R.S., A.V.D., and P.K.R.P. wrote the original draft., M.R.S., A.V.D., P.K.R.P performed review and editing of the original draft.

References

- (1) Nagy, Z. K.; Braatz, R. D. Advances and new directions in crystallization control. *Annu Rev Chem Biomol Eng* **2012**, *3* (1), 55-75. DOI: 10.1146/annurev-chembioeng-062011-081043 (accessed 2022/03/12).
- (2) Han, Q.; Brown, S. J.; Drummond, C. J.; Greaves, T. L. Protein aggregation and crystallization with ionic liquids: Insights into the influence of solvent properties. *J Colloid Interface Sci* **2022**, *608* (Pt 2), 1173-1190. DOI: 10.1016/j.jcis.2021.10.087.
- (3) Mangin, D.; Puel, F.; Veesler, S. Polymorphism in processes of crystallization in solution: a practical review. *Organic Process Research & Development* **2009**, *13* (6), 1241-1253.
- (4) Haase, F.; Lotsch, B. V. Solving the COF trilemma: towards crystalline, stable and functional covalent organic frameworks. *Chem Soc Rev* **2020**, *49* (23), 8469-8500. DOI: 10.1039/d0cs01027h.
- (5) Stock, N.; Biswas, S. Synthesis of Metal-Organic Frameworks (MOFs): Routes to Various MOF Topologies, Morphologies, and Composites. *Chemical Reviews* **2012**, *112* (2), 933-969. DOI: 10.1021/cr200304e.
- (6) Kondepudi, D. K.; Bullock, K. L.; Digits, J. A.; Yarborough, P. D. Stirring Rate as a Critical Parameter in Chiral-Symmetry Breaking Crystallization. *Journal of the American Chemical Society* **1995**, *117* (1), 401-404. DOI: DOI 10.1021/ja00106a045.
- (7) Myerson, A. S. *Handbook of industrial crystallization*; Butterworth-Heinemann, 2002.
- (8) Brittain, H. G. Polymorphism in pharmaceutical solids. *Drugs and the pharmaceutical sciences* **1999**, *95*, 183-226.
- (9) Wantha, L. Determination of Nucleation and Growth Mechanisms of the B Polymorph of L-Histidine by Induction Time Measurement. *Chem Eng Technol* **2016**, *39* (7), 1289-1294, https://doi.org/10.1002/ceat.201600045. DOI: 10.1002/ceat.201600045 (accessed 2022/03/15).
- (10) Izmailov, A. F.; Myerson, A. S.; Arnold, S. A statistical understanding of nucleation. *Journal of Crystal Growth* **1999**, *196* (2-4), 234-242.
- (11) Singh, M. R.; Ramkrishna, D. Dispersions in crystal nucleation and growth rates: Implications of fluctuation in supersaturation. *Chemical Engineering Science* **2014**, *107*, 102-113.
- (12) De Yoreo, J. J.; Vekilov, P. G. Principles of crystal nucleation and growth. *Reviews in mineralogy and geochemistry* **2003**, *54* (1), 57-93.
- (13) Yu, Z. Q.; Chew, J. W.; Chow, P. S.; Tan, R. B. H. Recent advances in crystallization control An industrial perspective. *Chemical Engineering Research & Design* **2007**, *85* (A7), 893-905. DOI: 10.1205/cherd06234.
- (14) Iwamatsu, M. Nucleation and growth of a core-shell composite nucleus by diffusion. *Phys Rev E* **2017**, *95* (4-1), 042803. DOI: 10.1103/PhysRevE.95.042803.
- (15) Diao, H.; Salazar, R.; Kelton, K. F.; Gelb, L. D. Impact of diffusion on concentration profiles around near-critical nuclei and implications for theories of nucleation and growth. *Acta Mater* **2008**, *56* (11), 2585-2591. DOI: 10.1016/j.actamat.2008.01.044.
- (16) Roelands, C. P. M.; Jiang, S. F.; Kitamura, M.; ter Horst, J. H.; Kramer, H. J. M.; Jansens, P. J. Antisolvent crystallization of the polymorphs of L-histidine as a function of

- supersaturation ratio and of solvent composition. *Cryst Growth Des* **2006**, *6* (4), 955-963. DOI: 10.1021/cg050529d.
- (17) Erdemir, D.; Lee, A. Y.; Myerson, A. S. Nucleation of crystals from solution: classical and two-step models. *Accounts of chemical research* **2009**, *42* (5), 621-629.
- (18) Coliaie, P.; Prajapati, A.; Ali, R.; Korde, A.; Kelkar, M. S.; Nere, N. K.; Singh, M. R. Machine Learning-Driven, Sensor-Integrated Microfluidic Device for Monitoring and Control of Supersaturation for Automated Screening of Crystalline Materials. *ACS Sens* **2022**, *7* (3), 797-805. DOI: 10.1021/acssensors.1c02358.
- (19) Coliaie, P.; Kelkar, M. S.; Nere, N. K.; Singh, M. R. Continuous-flow, well-mixed, microfluidic crystallization device for screening of polymorphs, morphology, and crystallization kinetics at controlled supersaturation. *Lab Chip* **2019**, *19* (14), 2373-2382, 10.1039/C9LC00343F. DOI: 10.1039/c9lc00343f.
- (20) Leng, J.; Salmon, J. B. Microfluidic crystallization. *Lab Chip* **2009**, *9* (1), 24-34. DOI: 10.1039/b807653g.
- (21) Shi, H. H.; Xiao, Y.; Ferguson, S.; Huang, X.; Wang, N.; Hao, H. X. Progress of crystallization in microfluidic devices. *Lab Chip* **2017**, *17* (13), 2167-2185. DOI: 10.1039/c6lc01225f.
- (22) Hall, K. W.; Sirk, T. W.; Klein, M. L.; Shinoda, W. A coarse-grain model for entangled polyethylene melts and polyethylene crystallization. *J Chem Phys* **2019**, *150* (24), 244901. DOI: 10.1063/1.5092229.
- (23) Toth, G. I.; Granasy, L.; Tegze, G. Nonlinear hydrodynamic theory of crystallization. *J Phys Condens Matter* **2014**, *26* (5), 055001. DOI: 10.1088/0953-8984/26/5/055001.
- (24) Luo, C. F.; Sommer, J. U. Coding coarse grained polymer model for LAMMPS and its application to polymer crystallization. *Computer Physics Communications* **2009**, *180* (8), 1382-1391. DOI: 10.1016/j.cpc.2009.01.028.
- (25) Cacciuto, A.; Frenkel, D. Simulation of colloidal crystallization on finite structured templates. *Phys Rev E Stat Nonlin Soft Matter Phys* **2005**, 72 (4 Pt 1), 041604. DOI: 10.1103/PhysRevE.72.041604.
- (26) Palberg, T. Crystallization kinetics of colloidal model suspensions: recent achievements and new perspectives. *J Phys Condens Matter* **2014**, *26* (33), 333101. DOI: 10.1088/0953-8984/26/33/333101.
- (27) Vettorel, T.; Meyer, H. Coarse Graining of Short Polythylene Chains for Studying Polymer Crystallization. *J Chem Theory Comput* **2006**, *2* (3), 616-629. DOI: 10.1021/ct0503264.
- (28) Alessandri, R.; Barnoud, J.; Gertsen, A. S.; Patmanidis, I.; de Vries, A. H.; Souza, P. C.; Marrink, S. J. Martini 3 Coarse-Grained Force Field: Small Molecules. *Advanced Theory and Simulations* **2022**, *5* (1), 2100391.
- (29) Conway, O.; An, Y.; Bejagam, K. K.; Deshmukh, S. A. Development of transferable coarse-grained models of amino acids. *Molecular Systems Design & Engineering* **2020**, *5* (3), 675-685.
- (30) Bialke, J.; Speck, T.; Lowen, H. Crystallization in a dense suspension of self-propelled particles. *Phys Rev Lett* **2012**, *108* (16), 168301. DOI: 10.1103/PhysRevLett.108.168301.
- (31) Lowen, H.; Palberg, T.; Simon, R. Dynamical criterion for freezing of colloidal liquids. *Phys Rev Lett* **1993**, 70 (10), 1557-1560. DOI: 10.1103/PhysRevLett.70.1557.

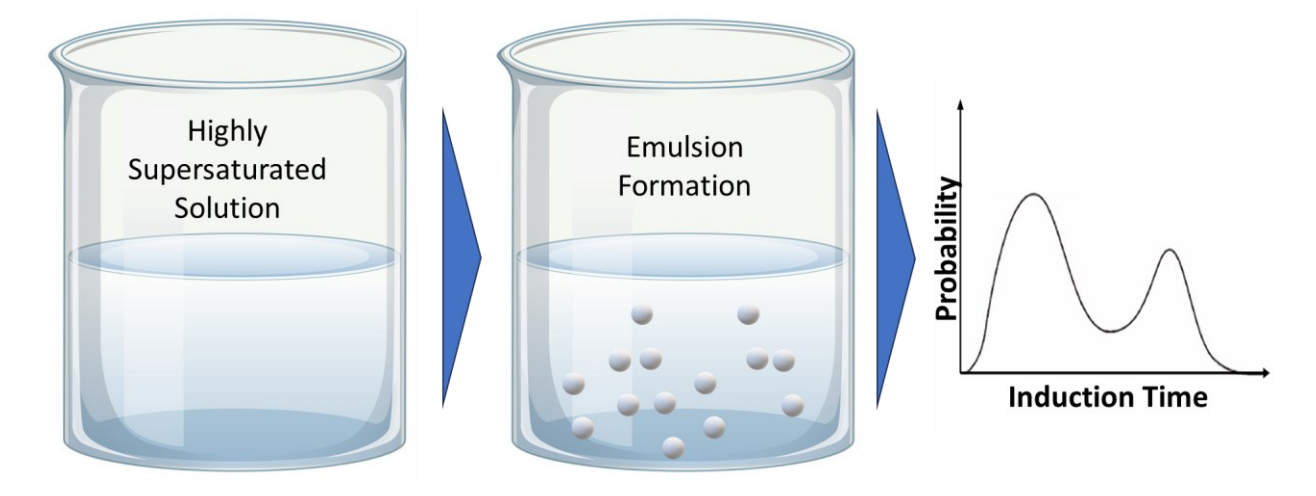
- (32) Sanz, E.; Marenduzzo, D. Dynamic Monte Carlo versus Brownian dynamics: A comparison for self-diffusion and crystallization in colloidal fluids. *J Chem Phys* **2010**, *132* (19), 194102. DOI: 10.1063/1.3414827.
- (33) Joswiak, M. N.; Doherty, M. F.; Peters, B. Ion dissolution mechanism and kinetics at kink sites on NaCl surfaces. *P Natl Acad Sci USA* **2018**, *115* (4), 656-661. DOI: 10.1073/pnas.1713452115.
- (34) Dighe, A. V.; Singh, M. R. Solvent fluctuations in the solvation shell determine the activation barrier for crystal growth rates. *P Natl Acad Sci USA* **2019**, *116* (48), 23954-23959, Article. DOI: 10.1073/pnas.1910691116.
- (35) von Ragué Schleyer, P.; Schreiner, P. R.; Schaefer III, H. F.; Jorgensen, W. L.; Thiel, W.; Glen, R. C.; Allinger, L. N.; Clark, T.; Gasteiger, J.; Chandler, D. Encyclopedia of computational chemistry. **1998**.
- (36) Abraham, M. J. GROMACS: High performance molecular simulations through multi-level parallelism from laptops to supercomputers. *SoftwareX* **2015**, *1*–2, 19.
- (37) Dighe, A. V.; Podupu, P. K. R.; Coliaie, P.; Singh, M. R. Three-Step Mechanism of Antisolvent Crystallization Published as part of a Crystal Growth & Design virtual special issue on Emerging Investigators 2022. *Cryst Growth Des* **2022**, *22* (5), 3119-3127. DOI: 10.1021/acs.cgd.2c00014.
- (38) Dighe, A. V.; Coliaie, P.; Podupu, P. K. R.; Singh, M. R. Selective desolvation in two-step nucleation mechanism steers crystal structure formation. *Nanoscale* **2022**, *14* (5), 1723-1732, 10.1039/D1NR06346D. DOI: 10.1039/d1nr06346d.
- (39) Novelli, G.; Maynard-Casely, H. E.; McIntyre, G. J.; Warren, M. R.; Parsons, S. Effect of high pressure on the crystal structures of polymorphs of l-histidine. *Cryst Growth Des* **2020**, *20* (12), 7788-7804.
- (40) Raza, S. A.; Schacht, U.; Svoboda, V.; Edwards, D. P.; Florence, A. J.; Pulham, C. R.; Sefcik, J.; Oswald, I. D. Rapid continuous antisolvent crystallization of multicomponent systems. *Cryst Growth Des* **2018**, *18* (1), 210-218.
- (41) Kelton, K. F.; Greenwood, G. W.; Greer, A. L.; Herlach, D. M.; Kelton, K. F. Diffusion—influenced nucleation: a case study of oxygen precipitation in silicon. *Philosophical Transactions of the Royal Society of London. Series A: Mathematical, Physical and Engineering Sciences* **2003**, *361* (1804), 429-446. DOI: 10.1098/rsta.2002.1138.
- (42) Braatz, R. D.; Hasebe, S. Particle size and shape control in crystallization processes. In *AIChE Symposium Series*, 2002; New York; American Institute of Chemical Engineers; 1998: pp 307-327.
- (43) Coliaie, P.; Kelkar, M. S.; Langston, M.; Liu, C.; Nazemifard, N.; Patience, D.; Skliar, D.; Nere, N. K.; Singh, M. R. Advanced continuous-flow microfluidic device for parallel screening of crystal polymorphs, morphology, and kinetics at controlled supersaturation. *Lab Chip* **2021**, *21* (12), 2333-2342. DOI: 10.1039/d1lc00218j.
- (44) Mullin, J.; Söhnel, O. Expressions of supersaturation in crystallization studies. *Chemical Engineering Science* **1977**, *32* (7), 683-686.

For Table of Contents Use Only

Manuscript Title: Emulsification of Supersaturated Solutions Amplifies Induction Time Variation in Crystallization

Authors: Anish V. Dighe, Prem K.R. Podupu, and Meenesh R. Singh

Graphics:



Synopsis: A mechanism of microphase or emulsion formation in supersaturated solutions is identified. A large variation in induction time is experimentally observed for various organic crystals, whose origin is often associated with the stochastic nature of the nucleation process. Here we reveal that such variations in induction times can be attributed to a previously unrecognized consequence of emulsification in supersaturated solution.